Based on Heusler Alloy Films Upscaling of Thermomagnetic Generators

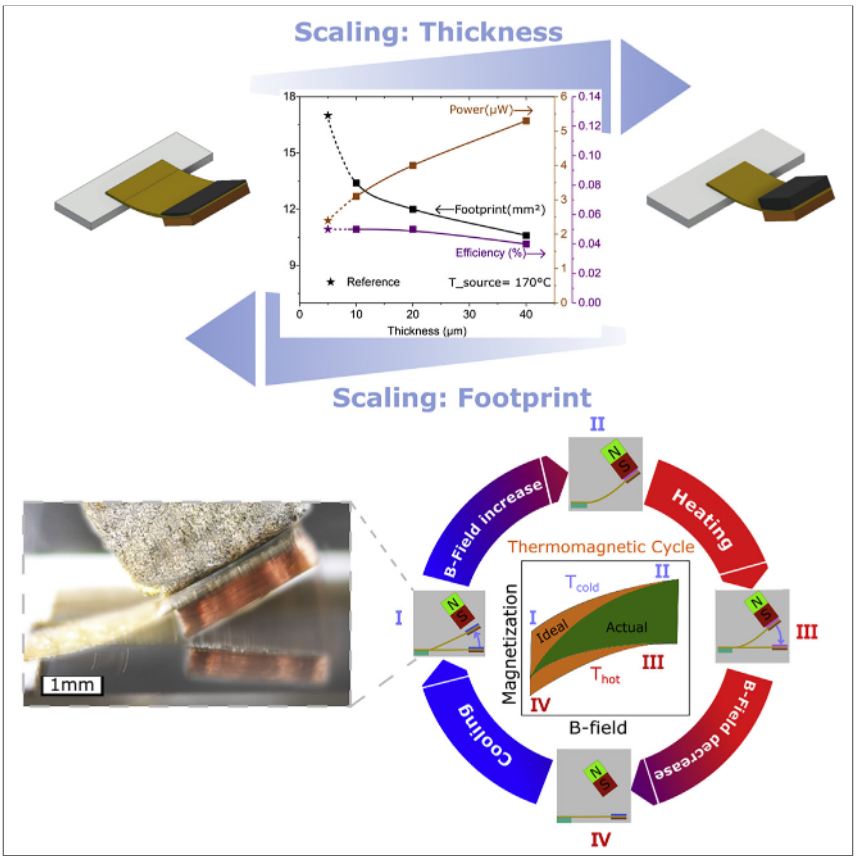

Joel Joseph, Makoto Ohtsuka, Hiroyuki Miki, Manfred Kohl

manfred.kohl@kit.edu

State-of-the-art thermomagnetic generators (TMGs) suffer from the limited temperature-dependent change of magnetization ΔM/ΔT and/or limited heat transfer dynamics. This shortcoming could be overcome by TMGs based on Heusler alloy films that exhibit large ΔM/ΔT and rapid heat transfer due to resonant self-actuation. Yet, power levels of individual devices are low, and upscaling becomes a key issue of material development and engineering. Here, we elucidate the heat transfer dynamics during resonant self-actuation and demonstrate how to optimize power output per footprint.

Upscaling of Thermomagnetic Generators Based on Heusler Alloy Films

Joel Joseph,[1] Makoto Ohtsuka,[2] Hiroyuki Miki,[3] and Manfred Kohl[1,4,*]

SUMMARY

Thermomagnetic (TM) generators based on Heusler alloy films have the potential to recover waste heat below 200°C at small temperature differences . Progress in the development of materials that exhibit large abrupt changes in ferromagnetic ordering and in film engineering enable efficient thermomagnetic generation via resonant self-actuation of freely movable film-based devices. Yet, power levels of individual devices are low, and upscaling becomes a key issue of material development and engineering. Here, we address the key question of how film thickness and device footprint affect power and efficiency. We investigate the scaling performance of heat intake, heat dissipation, and resulting local temperature changes. Based on this understanding, the electrical power per footprint could be increased by a factor of 3.4. Maximum values of electrical power per footprint are 50 μW/cm^2 at a temperature change of only 3°C, which marks an important milestone in the upscaling of Heusler alloy film-based TM generators.

INTRODUCTION

Energy harvesting has developed into a broad research area due to the widespread demand for energy in remote or hardly accessible places. Major applications are in wireless sensor networks, e.g., for environmental monitoring, in handheld or implantable devices as well as in wearable electronics to allow for self-sustaining operation without power supply by cables or batteries.[1,2] Recovery of thermal energy is of particular interest as waste heat is a growing and abundant energy resource. A large proportion of energy consumption in urban and industrial sectors is rejected as waste heat that increases with energy consumption. Much of this unrecovered waste heat energy is in the low temperature regime (10°C–250°C).[3–5] However, when temperature differences become small, energy conversion becomes inefficient. Thermoelectric generation using the Seebeck effect is currently the most mature technology for thermal energy generation in this temperature range.[6,7] However, thermoelectric generators suffer from restrictions of down-scaling and require relatively large temperature differences of at least 100°C to reach an efficiency of 5%.[6] The efficiency is determined by the thermoelectric figure of merit ZT, which is in the order of 1 for common thermoelectrics like bismuth telluride.[8]

Thermomagnetic (TM) generation has gained renewed interest in recent years, even though first concepts have been proposed already in the nineteenth century and various theoretical and experimental investigations on the use of ferromagnetic materials have been undertaken since then including cobalt (Co), iron (Fe), and gadolinium (Gd).[3,4,9] While relative efficiencies of ferromagnetic materials operating about their Curie temperature reach theoretical values up to 55% of Carnot efficiency,[10] experimental values are considerably smaller.[3,11] The different concepts

Context & Scale

Waste heat is a growing and abundant energy resource, particularly at low temperature below 200°C, which is difficult to recover by existing energy conversion technologies. Progress in the development of films that exhibit large abrupt changes in magnetization and rapid heat transfer unclose the development of thermodynamically efficient thermomagnetic generators. Detailed experiments and lumped element simulations for the case of Heusler alloy film Ni-Mn-Ga show that scaling of film thickness and device footprint oppositely affect power output. Based on this understanding, we could increase the electrical power per footprint by a factor of 3.4 for increasing film thickness from 5 to 40 μm reaching values of 50 μW/cm^2 at a temperature change of only 3°C. These results pave the way for the development of advanced generators consisting of parallel architectures with tailored footprint and films operating well below 100°C that open up waste heat recovery near room temperature.

focus either on first or second-order phase transformations near the Curie point and, more recently, consider spin reorientation that exploits a temperature-induced change in the magnetic easy axis.[12] Recent developments of macroscale TM demonstrators include thermomagnetic oscillators and linear harvesters.[13,14] A survey of thermomagnetic alloys with respect to energy per cycle and frequency has been reported.[15] Existing TM demonstrators either involve indirect energy conversion via periodic mechanical motion such as rotation and oscillation or direct thermal-to-magnetic energy conversion.[3] Major challenges arise due to the need for special materials that exhibit a large change of magnetization ΔM at small temperature difference ΔT and due to various engineering issues related to the strong thermo-magneto-mechanical coupling of system properties and various loss mechanisms, including magnetic stray fields, parasitic heat transfer, and friction. Experiments on a millimeter-scale TM energy harvesting device indicate that micro/nanoscale systems have the potential to operate at substantially higher frequencies due to increased surface-to-volume ratio allowing to generate higher power outputs.[16]

Recent progress in the development of Heusler alloys enables large, abrupt changes of magnetization in the vicinity of room temperature offering new opportunities to convert thermal to electrical energy.[15,17–21] Even for small magnetic fields of 24 kA m ^{1} (3 kOe) and small temperature difference ΔT of 5 K, calculations predict efficiencies in the order of 16% of the Carnot limit.[17,18] Heusler alloys offer a number of options for TM generation.[17,19] For instance, a first-order transformation from ferromagnetic austenite phase to nonferromagnetic martensite phase could be used in metamagnetic alloys such as Ni-Co-Mn-Z (Z = In, Sn).[17,22] Here, we make use of the abrupt drop of magnetization at the second-order ferromagnetic transition of the Heusler alloy film $Ni_{53.5}Mn_{23.8}Ga_{22.7}$, which will be referred to as Ni-Mn-Ga film hereinafter. The chemical composition is tailored to adjust phase transformation temperatures. The advantage of using a first-order magneto-structural transformation is the larger ΔM/ΔT. However, it comes with a hysteresis, which is absent for the second-order transition. Therefore, it highly depends on ΔM/ΔT and the hysteresis of the used material, which option may result in a higher power output.

In this work, the unique concept of TM generation via resonant self-actuation of a film cantilever is used, which allows for high frequency in the order of 100 Hz and, thus, rapid heat transfer.[20] By this approach, a high power density normalized to the active material volume of 120 mWcm ^{3} has been achieved,[20] which is in line with theoretical predictions of up to 300 mWcm ^{3} for thin plates.[17] Being a self-actuating and self-adjusting device, there is no external actuation or influence needed for operation except the thermal energy source. Yet, owing to the small volume of the active material of 2×2×0.005 mm^3, the power has been limited to about 2.4 μW.[20] Therefore, upscaling of the active material's volume will be essential to meet power levels for applications at length scales beyond the millimeter scale, while keeping the advantages of high efficiency and rapid heat transfer of film-based devices.

In the following, we investigate the scaling effects of Ni-Mn-Ga film thickness and the footprint of the TM generators on power and efficiency. Major challenges are in film fabrication maintaining the large change of magnetization ΔM at small temperature difference ΔT as well as in TM generator engineering enabling resonant operation conditions despite the increase of the active material's volume. We elucidate the heat transfer dynamics during resonant operation and demonstrate how to optimize power per footprint, which allows evaluating the potential of Heusler alloy film-based TM generation.

[1]Institute of Microstructure Technology, Karlsruhe Institute of Technology (KIT), Postfach 3640, 76021 Karlsruhe, Germany

[2]Institute of Multidisciplinary Research for Advanced Materials, Tohoku University, Sendai 980-8577, Japan

[3]Institute of Fluid Science, Tohoku University, Sendai 980-8577, Japan

[4]Lead Contact

*Correspondence: manfred.kohl@kit.edu

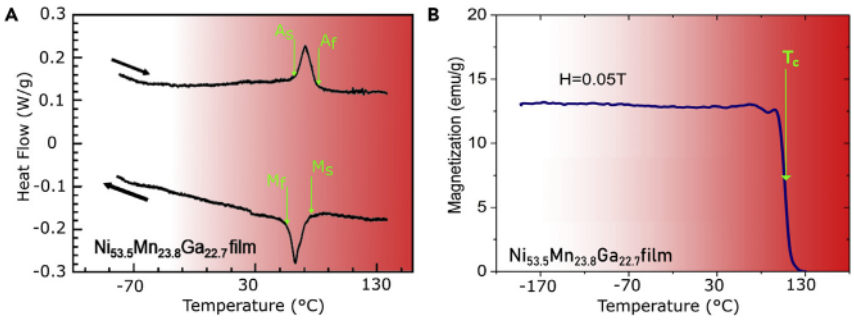

Figure 1. Thermal and Magnetic Characteristics of a Heusler Alloy Film Ni-Mn-Ga

(A) Differential scanning calorimetry measurement of a $Ni_{53.5}Mn_{23.8}Ga_{22.7}$ film with 5 μm thickness. The peaks reflect the first-order martensitic transformation with corresponding martensite start/finish temperatures $M_{s/f}$ of 74°C /57°C and austensite start/finish temperatures $A_{s/f}$ of 63°C/83°C.

(B) Low-field magnetization versus temperature curve upon heating for a $Ni_{53.5}Mn_{23.8}Ga_{22.7}$ film with 5 μm thickness. At the Curie temperature T_C of 102°C, the magnetization shows a sharp drop ΔM in a narrow temperature window ΔT.

HEUSLER Alloy Films

Heusler alloys are ordered intermetallics that exhibit multiferroic phase transformations as electronic spin interactions strongly depend on changes in interatomic distances and local symmetry.[23–26] Prominent examples are the alloys Ni-Mn-Z and Ni-Co-Mn-Z (Z = Ga, In, Sn, etc.) that exhibit giant effects including magnetic-field-induced strain,[24] magnetoresistance,[27] magnetocaloric effect,[28] and magnetic-field-induced shape memory effect.[26] Here, we focus on films of the magnetic shape memory alloy (MSMA) Ni-Mn-Ga, which show both, a first-order martensitic transformation and a second-order ferromagnetic transition. The Ni-Mn-Ga films are fabricated by RF magnetron sputtering, whereby the sputtering power is adjusted to control the Ni content and thus the phase transformation temperatures.[29] Film thickness is limited to a maximum of about 10 μm due to constraints in sputtering time and related film homogeneity. Heat treatment conditions are tailored for optimal temperature-dependent magnetization near the ferromagnetic transition. Phase transformation temperatures of the films are determined by differential scanning calorimetry (DSC). A typical DSC measurement is depicted in Figure 1A. The peaks reflect the first-order martensitic transformation with transformation temperatures in the range of 57°C– 83°C. The transition temperatures depend largely on chemical composition and related electron concentration per atomic unit (e/a-ratio), which allows tailoring in a wide range.[30] Figure 1B shows a temperature-dependent magnetization measurement of a Ni-Mn-Ga film at a low magnetic field of 0.05 T. At room temperature, the material is in a martensitic and ferromagnetic state. A small step-like feature occurs at about 70°C, which is attributed to the martensitic phase transformation. At the Curie temperature T_C of about 102°C, the magnetization undergoes an abrupt ferromagnetic transition showing a large change ΔM in a narrow temperature window ΔT, which is much less affected by chemical composition.[31] This transition exhibits no hysteresis due to its second-order nature. In the following, we use the abrupt change of $\Delta M/\Delta T$ at T_C to generate a temperature-dependent force for resonant self-actuation of the film cantilever in a magnetic field gradient at a low magnetic field (<0.5T). Under such conditions of a low magnetic field and well-separated first and second-order transitions, the magnetocaloric effect is assumed negligible.

Layout and Concept of UPSCALING

Figure 2A shows a schematic of the TM generator and illustrates the operation principle as well as the concept of upscaling. The TM generator consists of a

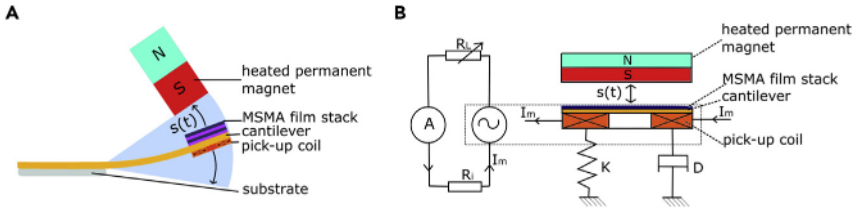

Figure 2. Layout and Modeling Approach

(A) Schematic operation principle of the TM generator. The MSMA film stack consists of one or several Ni-Mn-Ga films of 10 µm thickness separated by bonding layers. A heated permanent magnet is used as the magnetic field and heat source.

(B) Equivalent circuit diagram of the electro-mechanical part of the TM generator. The mechanical part consists of a spring-mass-damper system with stiffness K and damping constant D. The electrical part includes the internal resistances of the pick-up coil R_i and load resistance R_L. The induced electrical current is denoted by I_m.

freestanding metal cantilever beam of Cu-Zn that is mounted at one end to a substrate. The Ni-Mn-Ga film and a miniature pick-up coil are attached to the movable front end of the cantilever. A heatable permanent magnet of Samarium Cobalt (SmCo) is mounted above the cantilever front to generate a magnetic force. The magnet provides the magnetic field gradient needed to attract the cantilever front and, at the same time, acts as the heat source of the generator. While in ferromagnetic state, the cantilever is deflected out-of-plane toward the magnet, which heats the film during contact and induces the ferromagnetic transition. Thereby, the magnetic attraction force decreases, while the elastic force of the cantilever takes over and pulls the cantilever back. Thus, the antagonism of magnetic and elastic forces causes continuous self-actuation. An oscillatory motion of the cantilever occurs, which is supported by the inertia force of the cantilever front. The oscillation effectively enhances the cooling of the Ni-Mn-Ga film required to repeat the actuation cycle. In previous work, we demonstrated that resonant self-actuation is possible if heat transfer is large enough to cause a sufficiently large change of magnetization during oscillation.[20] By this unique concept of TM generation, the Ni-Mn-Ga film undergoes a continuous thermomagnetic cycle, whereby thermal energy is converted indirectly into magnetic energy via the generation of work. Both, the thermally and motion-induced change of magnetization induce a current in the pick-up coil according to Faraday's law. The range of heat source temperatures is determined by the Curie temperature T_C and the dynamics of heat transfer. The present layout is optimized for resonant operation between 130°C and 170°C.

For upscaling, the volume of the active material of the TM generator is increased in order to increase the power per footprint, which is an important figure of merit as the surface area is a key parameter for heat transfer. Three demonstrators are considered having a Ni-Mn-Ga film thickness of 10, 20, and 40 µm. However, film thicknesses are limited to a maximum of about 10 µm due to constraints in sputtering time and related film homogeneity. Therefore, we increase the thickness stepwise by stacking identical Ni-Mn-Ga films of 10 µm thickness with the same lateral dimensions and magnetization characteristics above each other as sketched in Figure 2A. Fixation of the film stack is accomplished by using bonding layers of conductive adhesive in between the films and an insulating layer between film stack and cantilever. The effect of the bonding layers will be considered in Discussion section. Increasing thermal and inertia mass upon upscaling affects the performance of the TM generator considerably. Therefore, a number of issues have to be solved in order to maintain the conditions of rapid heat transfer and resonant self-actuation. This includes fabrication technology, optimization of cantilever geometry affecting footprint, electrical load

resistance, and most importantly, heat intake during contact between the film stack and heat source (permanent magnet) as well as heat dissipation, which both depend on the dynamics of cantilever motion. The cantilever stiffness is adjusted by adapting the cantilever length. Thus, the scaling of film thickness is coupled to the footprint given by the lateral dimensions of cantilever and substrate. The footprint of the reference device of 5 μm thickness is 17 mm^2, which consists of the lateral dimensions of the cantilever of 3×5 mm^2 and of the substrate of 2 mm^2. The corresponding Ni-Mn-Ga film has lateral dimensions of 2×2 mm^2.[20] The magnetic attraction force is adjusted via the separation between magnet and cantilever front. A photo of the TM generator (Figure S1) can be found in the Supplemental Information. Figure 2B shows an equivalent circuit diagram of the TM generator. The mechanical part is represented by a spring-mass-damper system. The electrical part comprises the internal resistance of the pick-up coil, a variable load resistor, and current pre-amplifier.

Modeling Approach

A lumped element model (LEM) is set up to describe the heat transfer, dynamic motion, and resulting power generation. The simulation procedure and major analytic expressions are given in the Supplemental Information. As the mechanical, thermal, and magnetic properties of the TM generator are strongly coupled, the equation of motion needs to be solved simultaneously with the thermal kinetics and corresponding change of magnetic properties. The time-dependent temperature profile in the Ni-Mn-Ga film stack strongly affects the magnitude and phase dependency of the magnetic attraction force on the cantilever. The temperature profiles are determined by thermal LEM simulations, which is illustrated by a schematic diagram in Figure S2 in the Supplemental Information. The heat transfer between the Ni-Mn-Ga and bonding layers of the film stack is modeled using thermal resistors and thermal capacitors. The contact between film stack and the heat source is crucial for TM generation. The heat transfer between the film stack and surface of the magnet is determined by contact area and impact force during contact, which is included as a strongly repulsive elastic force. Thus, heat transfer is expected to increase for the increasing thickness of film stack as the increase of required cantilever stiffness and the increasing magnetic attraction force enlarge impact force. Since heat transfer coefficients critically depend on the dynamics of cantilever actuation, they are difficult to determine experimentally. Nevertheless, they can be determined by LEM simulations by matching simulated and experimental characteristics of frequency and stroke for each film thickness and heat source temperature. The obtained thickness dependence of heat transfer coefficients due to contact is summarized in Figure S3A in the Supplemental Information. The range of values is consistent with results obtained from the contact resistance equation showing that the used thermal boundary conditions are conservative.[32] Similarly, we assume thickness-dependent heat transfer coefficients for air convection. The obtained coefficients for convective heat transfer are summarized in Figure S3B. The field-dependent and temperature-dependent magnetization of the Ni-Mn-Ga films is determined experimentally and included in the model as a look-up table. The magnetic field, field gradient, and magnetic force are computed using analytical methods.[33] Calculated stationary magnetic forces are validated by experimental force-displacement characteristics. The dynamic mechanical deflection is described as a one-dimensional motion of the center-of-mass at the cantilever front by a spring-mass damper model. Dissipative forces are due to structural damping, viscous damping in air, and electromagnetic damping. The average electrical power is determined by the integration of the current signals induced in the pick-up coil. The load resistance is adjusted for maximum power, as shown in Figure S4 in the Supplemental Information.

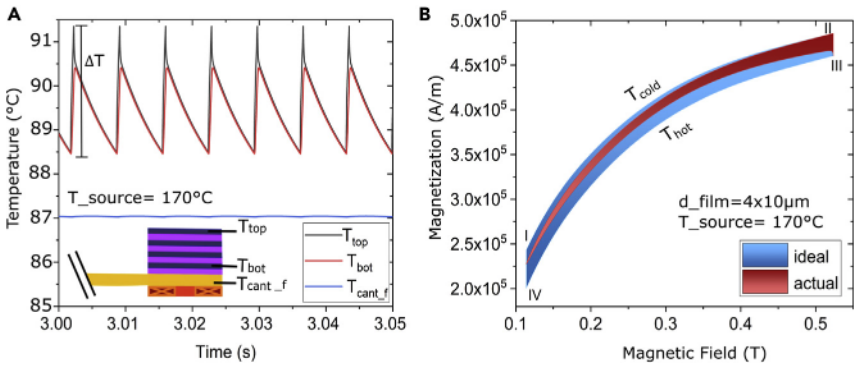

Figure 3. Thermomagnetic Cycle of the TM Generator

(A) LEM simulation of time-resolved average temperatures of top and bottom layer of the Ni-Mn-Ga film stack (T_{top} and T_{bot}) and of the cantilever front (T_{cant_f}) during thermomagnetic cycling of a demonstrator with overall Ni-Mn-Ga film thickness of 40 μm for a heat source temperature of 170°C. The maximum temperature change ΔT is indicated. The inset shows a schematic of the cantilever front with the MSMA film stack and pick-up coil.

(B) LEM simulation of actual and ideal thermomagnetic cycles of a demonstrator with Ni-Mn-Ga film thickness of 40 μm for a heat source temperature of 170°C. In ideal case, the cycles consist of four steps 1–4 as explained in the text. The enclosed areas are used to determine the generated magnetic energy.

Further details on the simulation procedure are presented in the Supplemental Information. The simulation parameters are summarized in Table S1. The LEM is validated by a series of experiments on time-dependent cantilever deflection and electrical performance. Typical simulated and experimental characteristics of resonant mechanical oscillation and corresponding electrical current induced in the pick-up coil are shown in Figure S5 in the Supplemental Information. For all film thicknesses and heat source temperatures studied, simulation characteristics agree with experimental results within an accuracy of 10%.

RESULTS

Dynamic Performance of Heat Transfer

Figure 3A shows simulated time-resolved average temperature profiles in the top and bottom layer of the Ni-Mn-Ga film stack, in the section of metal cantilever below the film stack and in the pick-up coil under stationary conditions for a heat source temperature of 170°C and an ambient temperature of 22°C. At the resonance frequency of 146 Hz, the top NiMnGa layer shows a temperature change ΔT of about 3°C between the maximum (T_{hot}) and minimum (T_{cold}) temperature. Subsequent Ni-Mn-Ga layers exhibit smaller temperature variations, as the bonding layers reduce heat transfer. Consequently, the bottom Ni-Mn-Ga layer only shows a temperature variation of about 2°C. The metal cantilever allows for conductive cooling of the film stack. In particular, the cantilever front below the bottom Ni-Mn-Ga layer acts as the main heat sink, i.e., its temperature (T_{cant_f}) represents the heat sink temperature. Under stationary conditions, this temperature reaches about 87°C showing only a minor temperature variation of 0.1°C. The pick-up coil shows an even smaller temperature variation in the order of 0.05°C due to its larger thermal capacitance.

Thermomagnetic Cycle

Figure 3B shows a simulated thermomechanical cycle for a demonstrator with film thickness of 40 μm in comparison with an idealized thermomechanical cycle. Under idealized conditions, four different steps can be distinguished: II→III and IV→I denote heating and cooling steps at fixed magnetic fields corresponding to the

ferromagnetic transition; I → II and III → IV assume that the change of magnetization for increasing and decreasing magnetic field occurs isothermally. The simulated cycle of the TM generator deviates from the idealized case due to non-isothermal magnetization change during oscillatory motion. After heating to its maximum temperature T_{hot}, the Ni-Mn-Ga film starts to cool once it moves away from the magnet and reaches its minimum temperature T_{cold} before touching the magnet again. The areas enclosed by the four steps define the net magnetic energy per cycle, which is reduced compared to the idealized cycle roughly by a factor of two. The magnetic energy per cycle is used to determine the magnetic power P_{mag} and efficiency η given by the ratio of magnetic power and net input heating power. In the present case of 40 μm film thickness shown in Figure 3B, the efficiency is determined to be about 0.041% under actual conditions. In the following, the effect of upscaling the Ni-Mn-Ga film thickness on average electrical power and efficiency will be evaluated.

Effect of Upscaling

Figure 4 gives an overview of the performance characteristics of the TM generators for increasing overall film thickness between 10 and 40 μm as well as various heat source temperatures between 130°C and 170°C. This is the most interesting temperature range for the investigated material, whereby the lower limit is determined by the material's Curie temperature. The upper limit depends on the design and could be extended further, which however appears to be less interesting from the point of view of harvesting waste heat.

For a given heat source temperature, the oscillation frequency and actuation stroke show a significant increase for increasing film thickness as shown in Figures 4A and 4B. The increase of oscillation frequency is a consequence of increased actuation forces and increased heat transfer. First, the cantilever stiffness increases as the cantilever length have to be reduced to counterbalance the increase of inertia mass for resonant operation. Second, the magnetic force increases due to the extra volume of magnetic material. The increasing actuation forces cause an increase in actuation stroke. In addition, they lead to an increase of impact force at contact to the magnet. Therefore, heat intake during contact Figure 4C also increases for increasing device thickness, which translates to a higher frequency of operation. At the same time, the footprint decreases with the decrease of the cantilever length. Similarly, the frequency increases for increasing heat source temperature as the transferred heat increases and, thus, the heating time during contact between cantilever front and heat source decreases. This change in heat transfer dynamics has a minor effect on the oscillation stroke, which changes by less than 20% for increasing heat source temperature as shown in Figure 4B.

The results on heat intake and maximum temperature changes ΔT are depicted in Figures 4C and 4D. Even though the transferred thermal energy during mechanical contact between cantilever front and the heat source is about the same for film thicknesses at the heat source temperature of 170°C, the heat intake increases for increasing film thickness due to the increasing inertia force. As shown in Figure 4C, the heat intake increases from 228 to 293.5 mW, when increasing the film thickness from 10 to 40 μm, respectively. On the other hand, the heat dissipation becomes less effective due to the larger film thickness and additional bonding layers, thus, more heating power is retained in the film stack. An overview of the conductive and convective heat losses for the different film thicknesses and heat source temperatures is given in Figures 4E and 4F.

Our LEM simulations reveal that heat losses due to conduction and convection increase for increasing heat source temperature as expected, however, they show

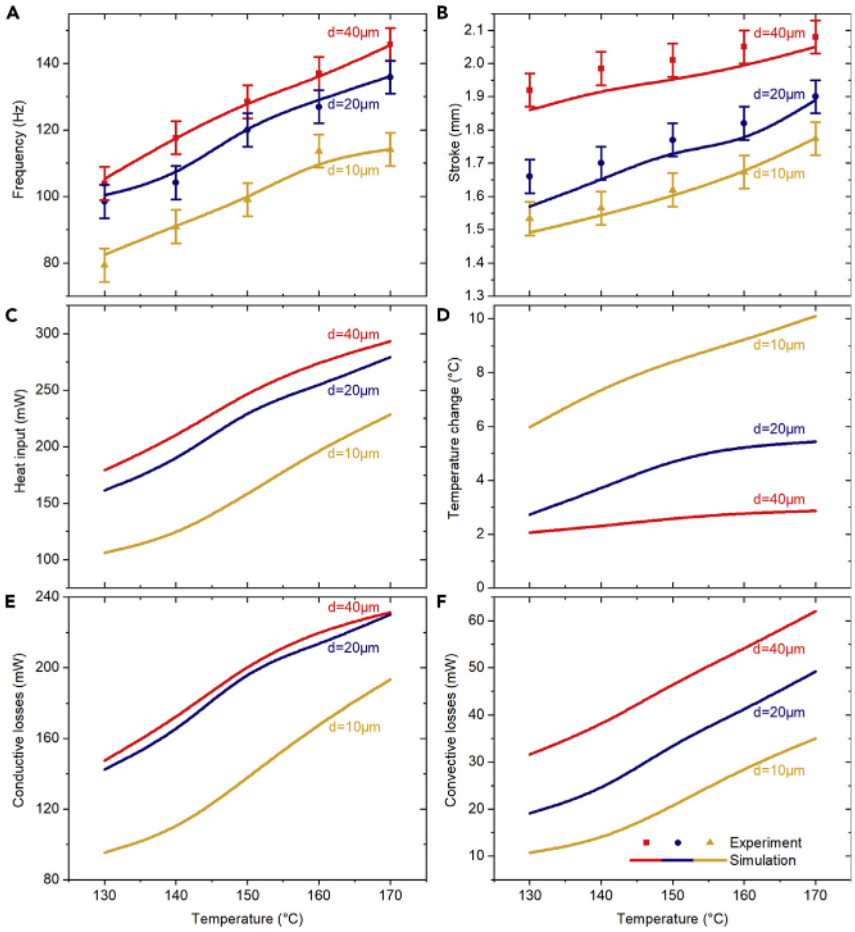

Figure 4. Effect of Upscaling on the Mechanical and Thermal Performance of TM Generators
(A) LEM simulation and experimental characteristics of oscillation frequency and (B) of the stroke of cantilever front. Experimental data are mean values with a standard error as indicated.
(C–F) (C) LEM simulation of heat intake, (D) of maximum temperature change of the MSMA film stack, (E) of conductive heat losses, and (F) of convective heat losses.
Thickness-dependent characteristics are plotted for different TM generators with Ni-Mn-Ga film thicknesses of 10, 20, and 40 µm as indicated.

different thickness dependencies. While convective heat losses are increasing continuously for increasing thickness, conductive heat losses approach an upper limit and saturate. A similar trend is found for lower heat source temperatures. The continuous increase in heat convection is due to the increasing oscillation frequency at increasing film thickness, while the increasing number of bonding layers pose an upper limit to heat conduction. Yet, heat conduction through the cantilever is the dominant mechanism for heat dissipation and the cantilever front acts as the main heat sink in all cases. As shown in Figure 3A for the case of 40 µm film thickness, the temperature at the cantilever front is almost constant during resonant oscillation. Similar behavior is found for smaller film thicknesses, while temperature values increase slightly from 87°C (40 µm) to 93°C (10 µm).

Both, heat intake and heat losses determine the maximum temperature change ΔT occurring in the top layer of the film stack, see Figures 3A and 4D. A detailed list of thickness-dependent temperature changes can be found in Table S2 in the Supplemental Information. For the case of 10 µm film thickness and a heat source

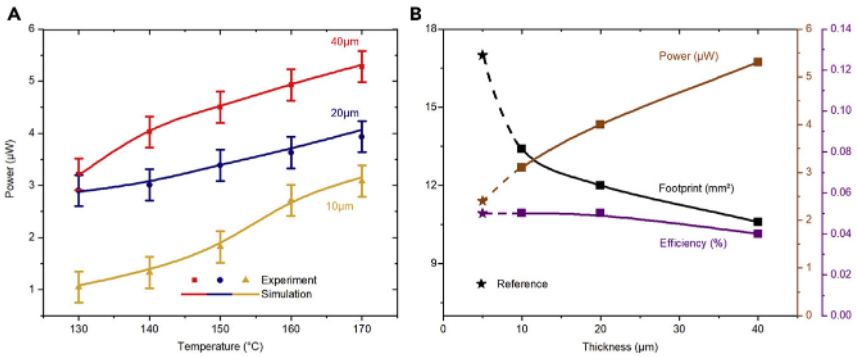

Figure 5. Scaling Effect of Film Thickness and Device Footprint on Power and Efficiency

(A) Simulated and experimental characteristics of average electrical power. Thickness-dependent characteristics are plotted for different TM generators with Ni-Mn-Ga film thicknesses of 10, 20 and 40 µm as indicated. Experimental data are mean values with a standard error as indicated.

(B) Interdependence of film thickness, device footprint, average electrical power, and efficiency. Film thickness and device footprint oppositely affect power. For comparison, the corresponding performance data of the reference device of 5 µm thickness are included, which have been evaluated for the same pick-up coil of 400 turns and heat source temperature of 170°C.

temperature of 170°C, the film temperature varies between about 101°C and 91°C corresponding to a ΔT of about 10°C. For increasing film thickness, ΔT decreases to 5.4°C and 2.9°C at film thicknesses of 20 and 40 µm, respectively. Thereby, mainly the maximum temperature in the film stack decreases, while the corresponding minimum temperature is almost unaffected. These temperature changes are further decreasing for decreasing heat source temperatures. At heat source temperatures of 120°C and below, when the achievable ΔT drops below 3°C, the corresponding change of magnetization ΔM becomes too low to support resonant self-actuation.

Figure 5A reveals a significant increase in electrical power for increasing overall film thickness as well as for increasing heat source temperature, which correlates with the increase of oscillation frequency. This increase results from the frequency-dependent increase of induced electrical current due to Faraday's law. Figure 5B summarizes the effect of scaling film thickness and device footprint on power and efficiency. We find that film thickness and device footprint are interrelated and oppositely affect the generated electrical power. Consequently, the power per footprint increases significantly by a factor of 3.4 when increasing film thickness to 40 µm. At the same time, the efficiency remains almost constant.

For the investigated range of heat source temperatures, extending the range of film thicknesses beyond 40 µm does not lead to a further increase of power. Simulations for a film thickness of 50 µm reveal a further increase of frequency but a decrease of stroke resulting in a decrease of power compared to 40 µm film thickness. A typical power versus thickness plot can be found in Figure S6 in the Supplemental Information. For larger film thicknesses of 60 µm and beyond, resonant self-actuation is no longer possible due to the limited heat transfer dynamics.

DISCUSSION

Upscaling of TM generators based on Heusler alloy films should enable the increase of electrical power while keeping the advantages of high efficiency and rapid heat transfer. Here, we address the key question of how scaling of film thickness and device footprint affect power and efficiency.

For this purpose, the following issues are investigated and evaluated:

(1) Fabrication technology: The thickness of active ferromagnetic material should be increased in discrete steps without affecting the temperature-dependent magnetization characteristic $\Delta M/\Delta T$.
(2) Optimization of electrical power: an increase of electrical power per footprint is the main motivation of this investigation. By increasing the thickness of active ferromagnetic material and adapting the footprint of the cantilever, the electrical power should increase, while constraints of self-actuation force and heat transfer are expected to pose an upper limit. This gives rise to two additional issues:
(3) Resonant self-actuation is the key to achieve large power and high efficiency. Therefore, resonant oscillation conditions have to be upheld despite the increase of active material's volume and corresponding changes of the coupled magneto-mechanical and thermomechanical properties.
(4) Efficient heat transfer: a detailed understanding of heat intake and heat dissipation is required for tuning of efficiency and optimization of power.

In this investigation, we use a certain combination of state-of-the-art magnetic materials, i.e., active Heusler alloy Ni-Mn-Ga films and SmCo permanent magnet, to fabricate a series of demonstrators and to compare their performance properties without loss of generality. This approach involves a number of technological constraints like maximum film thickness (10 μm) and a limited number of coil turns, which are considered as fixed boundary conditions. In order to ensure comparability, the same permanent magnet with the same magnetic field gradient and the same pick-up coil is used for all demonstrators. Under such conditions, issue (1) can be fulfilled by stacking identical Ni-Mn-Ga films of 10 μm thickness above each other and using bonding layers of conductive adhesive in between them. The additional bonding layers affect heat transfer within the film stack and overall heat dissipation, which will be further discussed below. We demonstrate that the considered material parameters and technology constraints allow for power optimization, but also give rise to a limit in the upscaling of the TM generator. Nevertheless, depending on future progress in the field, our approach can be transferred to other enhanced magnetic materials and improved technology constraints to enable further upscaling.

The main results of demonstrator performance are summarized in Table 1 for a heat source temperature of 170°C. An important outcome of this investigation is the significant increase in electrical power for increasing film thickness up to 40 μm, while the footprint decreases at the same time (issue [2]). Consequently, the magnetic power per footprint determined from the magnetic cycle increases from 0.8 mW/cm^2 to a maximum of 1.1 mW/cm^2 for increasing film thickness from 10 to 20 μm. Further increase in film thickness to 40 μm results in a slight decrease to 1.05 mW/cm^2. This decrease correlates with a slight decrease in efficiency as the heat intake further increases with increasing film thickness. Yet, the electrical power generated by induction in the pick-up coil shows a continuous increase with film thickness and reaches a maximum of 5.3 μW at 40 μm thickness. The corresponding electrical power per footprint is 50 $\mu W/cm^2$. In this case, a periodic temperature change of only 3°C is required; see Figure 4D. Compared to the reference device of 5 μm film thickness, this is an increase by more than a factor of 3.4.[20] This performance competes with state-of-the-art thermoelectric generators at length scales in the cm range and low-temperature difference.[34]

The strategy to achieve the power increase relies on the tuning of magnetic attraction force, mechanical reset force, and heat transfer dynamics in order to uphold

Table 1. Performance Results of the TM Generators

Film Thickness (μm)	Footprint (mm^2)	Frequency (Hz)	Stroke (mm)	ΔT (K)	Magnetic Power per Footprint (mW/cm^2)	η(%)	Electrical Power (μW)
10	13.4	114	1.8	10.1	0.8	0.047	3.1
2 X 10	12	136	1.9	5.4	1.1	0.046	4
4 X 10	10.6	145	2.1	2.9	1.05	0.041	5.3
40[a]	10.6	146	2.1	3.2	1.23	0.045	5.7

Results are given for heat source temperature of 170°C. The footprint is determined from the difference areas of the cantilever and the substrate area of $2mm^2$.
[a]For comparison, the estimated performance of a TM generator with a 40 μm thick homogeneous Ni-Mn-Ga layer is included, which is based on LEM simulations.

resonant oscillation conditions (issue [3]). The achieved increase in power follows from the increase of the mechanical energy of oscillatory motion, which increases for increasing mass and frequency as long as resonant conditions are maintained and which, in turn, supports magnetic cycles with increasing changes of magnetic energy.

Our results demonstrate that, for a given ferromagnetic material and magnetic field gradient, the upscaling approach is ultimately limited by the heat transfer dynamics (issue [4]). For better understanding, detailed simulations are performed on the scaling dependence of heat intake, heat dissipation, and of the resulting temperature changes in the Ni-Mn-Ga layers. The heat transfer coefficients depend on the dynamics of cantilever actuation, which in turn depends on film thickness and heat source temperature. By matching the simulated and experimental characteristics, it has been possible to obtain a consistent set of heat transfer coefficients given in Figure S4 in the Supplemental Information, which are in line with typical values reported in the literature.[32] LEM simulations reveal that heat intake increases for increasing film thickness, while conductive heat losses being the dominant mechanism for heat dissipation saturate. Thus, the corresponding fraction of average retained to average input heating power increases from about 80 % to 94 % for increasing film thickness from 10 to 40 μm, respectively. At lower heat source temperatures, these fractions only deviate slightly and show the same thickness dependence. This result shows that a major fraction of heat remains in the SMA film stack and contributes to the temperature change ΔT, which is an important prerequisite for large power.

However, the increasing film thickness causes a decrease in temperature change ΔT of the film stack during oscillation, which has two important consequences. First, the decreasing ΔT leads to a reduction in efficiency for increasing film thickness. Second, the decreasing ΔT poses a critical limit on further upscaling of film thickness. The present investigation clearly reveals that a minimum ΔT is required for resonant self-actuation, which depends on the details of material properties, operation temperatures, and device design. For the present TM generators, this limit is in the range of 2°C–3°C. When the film thickness becomes too large, the achievable ΔT is no longer sufficient to cause enough change of magnetization ΔM to support resonant self-actuation.

An interesting question is concerned with the role of the bonding layers used in this study to stack several Ni-Mn-Ga films above each other. The bonding layers reduce heat transfer and, thus, cause a small temperature gradient from top to bottom (<1K) so that the bottom layers contribute less to resonant self-actuation. In order to analyze this effect, we performed a simulation, in which the stack of four Ni-Mn-Ga films and thermally conductive bonding layers have been replaced by one

40-μm-thick homogeneous Ni-Mn-Ga layer with just one remaining non-conductive bonding layer of thickness in the range of 15–20 μm. As can be seen in Table 1, removing the intermediate bonding layers slightly improves power. In the optimum case, an increase in electrical power and efficiency by about 10% is expected due to the better homogeneity of the temperature profile in the 40 μm thick layer. For smaller film thicknesses and lower heat source temperatures, these effects are even smaller. However, decreasing the thickness of the remaining bonding layer or increasing its thermal conductivity would significantly increase heat dissipation and, thus, power and efficiency would strongly decrease.

Reliability is no major concern as the Ni-Mn-Ga layers are not subjected to large strain and thermal changes remain small as well. So far, demonstrators were operated continuously for up to 3 days without any performance change corresponding to more than 3×10^6 operation cycles.

Conclusions

TM generators are moving into the focus of research on waste heat recovery due to recent progress in the development of Heusler alloys that exhibit large abrupt changes of magnetization at small temperature difference $\Delta M/\Delta T$ as well as in the development of thermodynamically efficient film-based devices that convert heat to electricity within a small temperature difference below 10°C. The high-performance operation is achieved by thermally induced resonant self-actuation at the large amplitude and high frequency using a film cantilever with a large surface-to-volume ratio. Here, investigated heat source temperatures are in the range between 130°C and 170°C, whereby the low-temperature limit is determined by the Curie temperature. We demonstrate how to enhance power by upscaling the active material's volume and, at the same time, keeping the advantages of high efficiency and rapid heat transfer of film-based devices. In particular, we show that the scaling of film thickness and device footprint oppositely affect power. Consequently, the electrical power per footprint of film-based TM generators can be enhanced by more than a factor of 3.4 when increasing the film thickness from 5 to 40 μm. Maximum values of electrical power per footprint are about 50 $\mu W/cm^2$ at a temperature change of only 3°C. This performance competes with state-of-the-art thermoelectric generators at miniature length scales (cm range). Below 3°C, resonant self-actuation is no longer possible due to the limited change of magnetization ΔM of the used film material.

The large power per footprint at low-temperature difference is of particular interest for miniature scale thermal energy harvesting to meet the growing needs, e.g., in wireless sensor networks and smart control systems for the building sector or industry 4.0. It is foreseen that upscaled TM generators could be arranged in parallel architectures to cover larger areas toward meter scale for waste heat recovery without giving up the rapid heat transfer due to the film geometry and keeping the condition of resonant self-actuation.

Further advances in the field strongly depend on progress in fabrication technology (e.g., extending maximum film thickness, increasing the number of coil turns at micrometer scale) and in further improvements of materials properties including magnetization change per temperature ($\Delta M/\Delta T$) and thermal conductivity. Heusler alloys showing first-order magneto-structural phase transformation are of special interest; however, the focus has to be on alloys with hysteresis close to zero. Another important direction of research should be dedicated to advanced Heusler alloy films

with Curie temperatures well below 100°C to enable waste heat recovery near room temperature.

EXPERIMENTAL PROCEDURES

Resource Availability

Lead Contact

Further information and requests for resources should be directed to and will be fulfilled by the Lead Contact, Manfred Kohl (manfred.kohl@kit.edu).

Materials Availability

There are restrictions on the availability of Ni-Mn-Ga films due to the lack of an external centralized repository for its distribution and our need to maintain the stock.

Data and Code Availability

The published article includes all datasets generated or analyzed during this study. The LEM supporting the current study has not been deposited in a public repository because it is used in on-going research, but it is available from the Lead Contact on request.

Fabrication

The Ni-Mn-Ga films are prepared by RF magnetron sputtering in a high-purity argon atmosphere. The sputtering power is adjusted to control the Ni content and thus the phase transformation temperatures.[29] Heat treatment is performed at 1,073 K for 10 h to tailor the temperature-dependent change of magnetization at the Curie temperature T_C. The composition of crystallized freestanding films is determined to be $Ni_{53.5}Mn_{23.8}Ga_{22.7}$ by the inductively coupled plasma method. The film thickness is adjusted by the sputtering time to be 5 and 10 μm. Details on the structure of the investigated films can be found in Ohtsuka et al.[35]

The cantilever beams are fabricated by cutting a brass (Cu-Zn) sheet of 20 μm thickness keeping a tolerance of less than 20 μm. Their lateral size and length are adjusted in each case to match the thickness of the Ni-Mn-Ga film. The Ni-Mn-Ga films are bonded above each other using conductive adhesive and are attached to the cantilever using non-conductive adhesive. The pick-up coils are fabricated by sandwiching a 250 μm thick Poly(methyl methacrylate) (PMMA) core of area 1 × 1 mm^2 in between two 25 μm Kapton foils of area 2 × 2 mm^2. The coils are wound with a self-made setup using an insulated copper wire with a diameter of 15 μm. A high-temperature permanent magnet of Samarium Cobalt (SmCo) with operating temperature tolerance up to 350°C is used as the magnetic field and heat source. It has a cross-sectional area of 3 × 3 mm^2 and an axially pole distance of 8 mm. The magnet is positioned with respect to the Ni-Mn-Ga film surface at an optimum distance and angle using a digital microscope to ensure maximum contact but to avoid impact to the magnet surface under operation. The magnet is heated until a stationary temperature is reached before experiments are started. Data are recorded by keeping the temperature of the heat source constant and changing the load resistance of each reading. These steps are repeated for each set of source temperature.

ACKNOWLEDGMENTS

This work was funded by the German Science Foundation (DFG) by the project "Thervest II" and partly supported by the Core-to-Core Program A "Advanced Research Networks" of the Japanese Science Foundation (JSPS). The authors would like to thank S. Fähler for critical reading of the manuscript.

AUTHOR CONTRIBUTIONS

J.J. designed and fabricated the TM generators, designed and performed the experiments, developed the simulation model, analyzed the data, and wrote the initial draft. M.O. designed and fabricated the Ni-Mn-Ga films and performed DSC and magnetization measurements. H.M. designed and optimized the Ni-Mn-Ga films. M.K. conceived the concept, designed the TM generators, supervised the experiments and simulations, and wrote the manuscript.

DECLARATION OF INTERESTS

The authors declare no competing interests. The authors have a patent related to this work.

REFERENCES

1. Matiko, J.W., Grabham, N.J., Beeby, S.P., and Tudor, M.J. (2014). Review of the application of energy harvesting in buildings. Meas. Sci. Technol. *25*, 012002.
2. Vullers, R., Schaijk, R., Visser, H., Penders, J., and Hoof, C. (2010). Energy harvesting for autonomous wireless sensor networks. IEEE Solid-State Circuits Mag. *2*, 29–38.
3. Kishore, R.A., and Priya, S. (2018). A review on design and performance of thermomagnetic devices. Renew. Sustain. Energy Rev. *81*, 33–44.
4. Bucsek, A.N., Nunn, W., Jalan, B., and James, R.D. (2020). Energy conversion by phase transformation in the small-temperature-difference regime. Annu. Rev. Mater. Res. *50*, 283–318.
5. Kitanovski, A. (2020). Energy applications of magnetocaloric materials. Adv. Energy Mater. *10*, 1903741.
6. Bierschenk, J.L. (2009). Thermoelectrics. In Energy Harvesting Technologies, S. Priya and D.J. Inman, eds. (Springer), pp. 337–350.
7. Min, G. (2010). Thermoelectric energy harvesting. In Energy Harvesting for Autonomous Systems, S.P. Beeby and N. White, eds. (Artech House)), pp. 135–155.
8. Snyder, G.J., and Toberer, E.S. (2008). Complex thermoelectric materials. Nat. Mater. *7*, 105–114.
9. Tesla, N. (1889). Thermo magnetic motor (US Patent), 396121.
10. Brillouin, L., and Iskenderian, H. (1948). Thermomagnetic generator. Electron. Commun *25*, 300–311.
11. Hsu, C.J., Sandoval, S.M., Wetzlar, K.P., and Carman, G.P. (2011). Thermomagnetic conversion efficiencies for ferromagnetic materials. J. Appl. Phys. *110*, 123923.
12. Wetzlar, K.P., Keller, S.M., Phillips, M.R., and Carman, G.P. (2016). A unifying metric for comparing thermomagnetic transduction utilizing magnetic entropy. J. Appl. Phys. *120*, 244101.
13. Deepak, K., Varma, V.B., Prasanna, G., and Ramanujan, R.V. (2019). Hybrid thermomagnetic oscillator for cooling and direct waste heat conversion to electricity. Appl. Energy *233–234*, 312–320.
14. Kishore, R.A., Singh, D., Sriramdas, R., Garcia, A.J., Sanghadasa, M., and Priya, S. (2020). Linear thermomagnetic energy harvester for low-grade thermal energy harvesting. J. Appl. Phys. *127*, 044501.
15. Deepak, K., Pattanaik, M.S., and Ramanujan, R.V. (2019). Figure of merit and improved performance of a hybrid thermomagnetic oscillator. Appl. Energy *256*, 113917.
16. Ujihara, M., Carman, G.P., and Lee, D.G. (2007). Thermal energy harvesting device using ferromagnetic materials. Appl. Phys. Lett. *91*, 1–4.
17. Srivastava, V., Song, Y., Bhatti, K., and James, R.D. (2011). The direct conversion of heat to electricity using multiferroic alloys. Adv. Energy Mater. *1*, 97–104.
18. Post, A., Knight, C., and Kisi, E. (2013). Thermomagnetic energy harvesting with first order phase change materials. J. Appl. Phys. *114*, 033915.
19. Gueltig, M., Ossmer, H., Ohtsuka, M., Miki, H., Tsuchiya, K., Takagi, T., and Kohl, M. (2014). High frequency thermal energy harvesting using magnetic shape memory films. Adv. Energy Mater. *4*, 1400751.
20. Gueltig, M., Wendler, F., Ossmer, H., Ohtsuka, M., Miki, H., Takagi, T., and Kohl, M. (2017). High-performance thermomagnetic generators based on Heusler alloy films. Adv. Energy Mater. *7*, 1601879.
21. Waske, A., Dzekan, D., Sellschopp, K., Berger, D., Stork, A., Nielsch, K., and Fähler, S. (2019). Energy harvesting near room temperature using a thermomagnetic generator with a pretzel-like magnetic flux topology. Nat. Energy *4*, 68–74.
22. Song, Y., Bhatti, K.P., Srivastava, V., Leighton, C., and James, R.D. (2013). Thermodynamics of energy conversion *via* first order phase transformation in low hysteresis magnetic materials. Energy Environ. Sci. *6*, 1315.
23. Webster, P.J., and Ziebeck, K.A.R. (1988). Heusler Alloys: Crystallographic Structure (Springer), pp. 75–184.
24. Ullakko, K., Huang, J.K., Kantner, C., O'Handley, R.C.O., and Kokorin, V.V. (1996). Large magnetic-field-induced strains in Ni2MnGa single crystals. Appl. Phys. Lett. *69*, 1966–1968.
25. Krenke, T., Acet, M., Wassermann, E.F., Moya, X., Mañosa, L., and Planes, A. (2005). Martensitic transitions and the nature of ferromagnetism in the austenitic and martensitic states of Ni-Mn-Sn alloys. Phys. Rev. B *72*, 1–9.

26. Kainuma, R., Imano, Y., Ito, W., Sutou, Y., Morito, H., Okamoto, S., Kitakami, O., Oikawa, K., Fujita, A., Kanomata, T., et al. (2006). Magnetic-field-induced shape recovery by reverse phase transformation. Nature *439*, 957–960.

27. Chernenko, V.A., Ohtsuka, M., Kohl, M., Khovailo, V.V., and Takagi, T. (2005). Transformation behavior of Ni-Mn-*Ga* thin films. Smart Mater. Struct. *14*, S245–S252.

28. Krenke, T., Duman, E., Acet, M., Wassermann, E.F., Moya, X., Mañosa, L., and Planes, A. (2005). Inverse magnetocaloric effect in ferromagnetic Ni-Mn-Sn alloys. Nat. Mater. *4*, 450–454.

29. Suzuki, M., Ohtsuka, M., Suzuki, T., Matsumoto, M., and Miki, H. (1999). Fabrication and characterization of sputtered Ni2MnGa thin films. Mater. Trans. JIM *40*, 1174–1177.

30. Chernenko, V.A. (1999). Compositional instability of β-phase in Ni-Mn-Ga alloys. Scr. Mater. *40*, 523–527.

31. Kohl, M., Krevet, B., Ohtsuka, M., Brugger, D., and Liu, Y. (2006). Ferromagnetic shape memory microactuators. Mater. Trans. *47*, 639–644.

32. Karwa, R. (2017). Thermal contact resistance. Heat Mass Transfer (Springer Nature), pp. 101–104.

33. Kohl, M., Gueltig, M., and Wendler, F. (2018). Coupled simulation of thermomagnetic energy generation based on NiMnGa Heusler alloy films. Shap. Mem. Superelasticity *4*, 242–255.

34. Nozariasbmarz, A., Collins, H., Dsouza, K., Polash, M.H., Hosseini, M., Hyland, M., Liu, J., Malhotra, A., Ortiz, F.M., Mohaddes, F., et al. (2020). Review of wearable thermoelectric energy harvesting: from body temperature to electronic systems. Appl. Energy *258*, 114069.

35. Ohtsuka, M., Sanada, M., Matsumoto, M., Takagi, T., and Itagaki, K. (2003). Shape memory behavior of Ni-Mn-*Ga* sputtered films under a magnetic field. Mater. Trans. *44*, 2513–2519.